

## RESEARCH LETTER

10.1002/2013GL058812

## Key Points:

- A set of three-dimensional GPS coseismic displacement data of Lushan earthquake is provided
- Rupture is dominated by thrust faulting with a significant sinistral component
- Main rupture is at 13 km depth, with moment release equivalent to Mw6.6 event

## Supporting Information:

- Readme
- Text file (including Tables S1 and S2).
- Figures S1–S7.
- Tables S3 and S4.

## Correspondence to:

M. Wang,  
mwang@gps.gov.cn

## Citation:

Jiang, Z., et al. (2014), GPS constrained coseismic source and slip distribution of the 2013 Mw6.6 Lushan, China, earthquake and its tectonic implications, *Geophys. Res. Lett.*, 41, doi:10.1002/2013GL058812.

Received 22 NOV 2013

Accepted 16 DEC 2013

Accepted article online 18 Dec 2013

## GPS constrained coseismic source and slip distribution of the 2013 Mw6.6 Lushan, China, earthquake and its tectonic implications

Zaisen Jiang<sup>1</sup>, Min Wang<sup>2</sup>, Yanzhao Wang<sup>2</sup>, Yanqiang Wu<sup>1</sup>, Shi Che<sup>3</sup>, Zheng-Kang Shen<sup>4</sup>, Roland Bürgmann<sup>5</sup>, Jianbao Sun<sup>2</sup>, Yonglin Yang<sup>6</sup>, Hua Liao<sup>6</sup>, and Qiang Li<sup>7</sup>

<sup>1</sup>CEA Key Laboratory of Earthquake Prediction, Institute of Earthquake Science, China Earthquake Administration, Beijing, China, <sup>2</sup>State Key Laboratory of Earthquake Dynamics, Institute of Geology, China Earthquake Administration, Beijing, China, <sup>3</sup>China Earthquake Administration, Beijing, China, <sup>4</sup>Department of Earth and Space Sciences, University of California, Los Angeles, California, USA, <sup>5</sup>Department of Earth and Planetary Science, University of California, Berkeley, California, USA, <sup>6</sup>Sichuan Earthquake Administration, Chengdu, China, <sup>7</sup>National Earthquake Infrastructure Service, China Earthquake Administration, Beijing, China

**Abstract** The 20 April 2013 Lushan earthquake occurred on the southern section of the Longmen Shan fault system. Using GPS data from 33 continuous stations, we derive a three-dimensional coseismic displacement field of the earthquake and invert for the location, geometry, and slip distribution of the fault rupture. Our study result indicates that the earthquake occurred on a reverse fault striking N28°E and dipping 43° to the NW, with the maximum slip located at 30.292°N, 102.943°E, and 13 km depth. The rupture is dominated by thrust faulting, with a slight but still statistically significant sinistral component. The seismic moment release is  $9.5 \times 10^{18}$  N·m, equivalent to a Mw6.6 earthquake. Our results suggest that at the southern end of the Longmen Shan fault zone near the triple junction with the Xianshuihe and Anninghe faults, the kinematic deformation field is no longer block-like, but broadly distributed to accommodate the buttressing effect of deformation around the fault triple junction.

### 1. Introduction

The Longmen Shan fault system is a tectonic block boundary separating the Sichuan basin from the eastern margin of the Tibetan plateau. Since the late Quaternary, tectonic deformation along this fault system has been dominated by thrust motion accompanied by a dextral strike-slip component [Burchfiel *et al.*, 1995; Densmore *et al.*, 2007]. Deformation rates across the fault system, however, are relatively low at 1 ~ 3 mm/a [King *et al.*, 1997; Chen *et al.*, 2000; Ma *et al.*, 2005; Shen *et al.*, 2005]. The 2008 Mw7.9 Wenchuan earthquake ruptured mostly the central section of the Longmen Shan fault system, and its aftershocks propagated toward the northern section of the fault system [Zhang *et al.*, 2008; Xu *et al.*, 2009]. The 20 April 2013 Lushan earthquake occurred on the southernmost section of the Longmen Shan fault system, with its epicenter located at 30.3°N, 103.0°E by China Earthquake Networks Center (CENC, <http://news.ceic.ac.cn/CC20130420080246.html>), and ~80 km southwest of the southwest end of the Wenchuan surface rupture [Xu *et al.*, 2009]. Estimates of the hypocenter and centroid depth range from 10 to 22 km [Zeng *et al.*, 2013] (Global GMT, <http://www.globalcmt.org>; CENC CMT, <http://news.ceic.ac.cn/CC20130420080246.html>; USGS CMT and W-phase CMT, <http://earthquake.usgs.gov/earthquakes/eqinthenews>), and the depths of aftershocks range from 7 to 25 km [Xu *et al.*, 2013].

The southern section of the Longmen Shan fault system consists of several imbricated reverse faults in an 80 km wide zone, including, from northwest to southeast, the Gengda-Longdong, Yanjing-Wulong, Shuangshi-Dachuan, and Dayi faults (Figure 1). Geological investigations following the Lushan earthquake, however, found no clear surface breaks along these active faults and adjacent areas, but only secondary faulting features, such as fissure cracks, soil liquefaction, and pushed-up cement pavement in the epicentral region [Xu *et al.*, 2013].

The focal mechanism solution from the Global CMT project indicates that the Lushan earthquake is primarily a reverse faulting event with a minor right-slip component on a fault plane striking N30°E and dipping 38° to the NW, with a seismic moment release of  $1.06 \times 10^{19}$  N·m, equivalent to a Mw6.6 event. The CENC CMT solution is

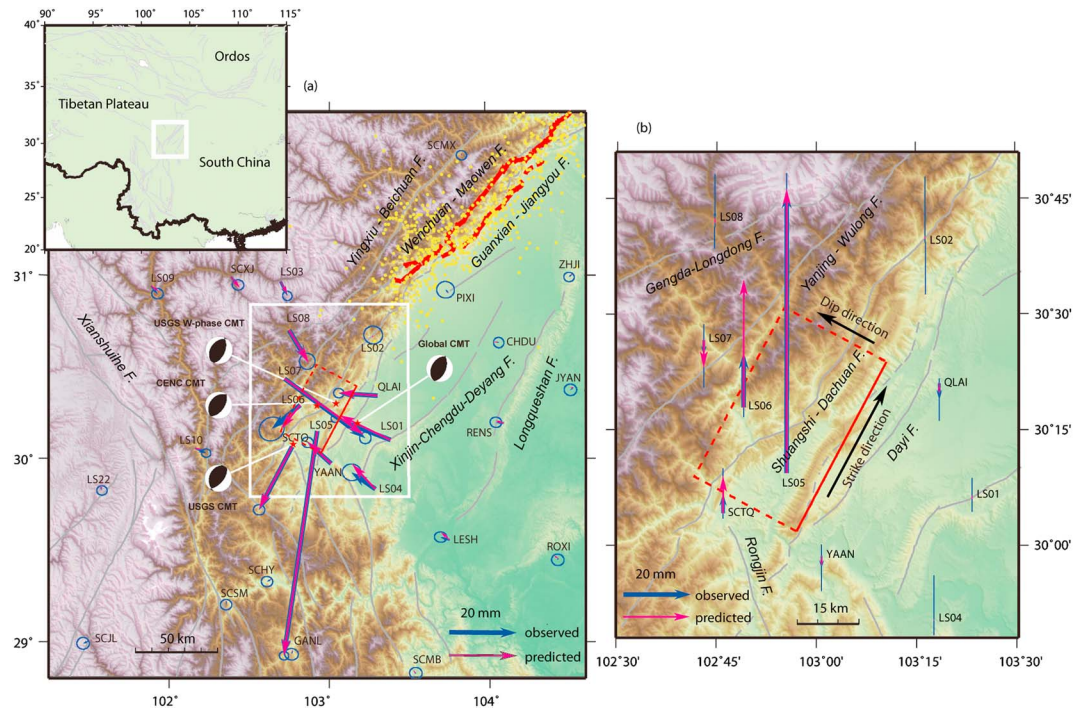


**Figure 1.** Tectonic setting of the Lushan earthquake and GPS data fitting. Light grey lines indicate regional faults, and dashed grey lines are inferred fault traces. The rectangle outlined by red lines marks the surface projection of the fault plane of the Lushan earthquake. (a) Red lines and yellow circles show surface rupture and aftershocks of the Wenchuan earthquake. CENC CMT, Global CMT, USGS W-phase CMT, and USGS CMT mechanism solutions and their centroid locations are also shown. Blue and Magenta arrows are GPS-observed and model-predicted horizontal coseismic displacements of the Lushan earthquake, respectively. (b) Blue and Magenta arrows are the observed and model-predicted vertical displacements of GPS sites located near the epicentral region. The uncertainties of GPS-observed displacements are represented as ellipses and vertical bars at arrow tips, indicating 70% confidence levels.

similar to the Global CMT solution, with a seismic moment release of  $1.60 \times 10^{19} \text{ N} \cdot \text{m}$ , equivalent to a Mw6.7 event. The USGS reported three moment tensor solutions, among which the body wave solution showed no significant strike-slip component, the W-phase solution yielded a dextral component with a rake angle of  $103^\circ$ , and the centroid moment solution revealed a sinistral component with a rake angle of  $71^\circ$ . A greater dip angle of  $47^\circ$  was obtained by Zeng *et al.* [2013] using regional P wave first-arrival data. Two rupture process studies of finite slip constrained by far-field waveform data also confirmed the reverse faulting mechanism, with the seismic moment release estimated as  $1.54 \times 10^{19} \text{ N} \cdot \text{m}$  and  $1.69 \times 10^{19} \text{ N} \cdot \text{m}$  [Wang *et al.*, 2013; Zhang *et al.*, 2013], equivalent to a Mw6.7 and Mw6.8 event, respectively. These differences in focal mechanisms, earthquake locations, and seismic moment estimates are not trivial and are intrinsically related to the differences in seismic data inversion approaches and data error. Geodetic crustal displacement data can provide independent constraints and thus improve the accuracy of focal parameter estimates, especially when no surface rupture is available to provide constraints on the fault geometry.

## 2. GPS Observed Coseismic Displacements

We collect GPS data from 33 continuous stations located within 200 km of the Lushan earthquake epicenter to obtain the coseismic deformation field of the quake, and the result is shown in Figure 1 (see the supporting information for details of GPS data collection and processing and quality of the result). Displacements at millimeter level or above are observed within 150 km from the epicenter. The largest displacement is observed at the site LS05, located ~15 km south of the epicenter, with ~68 mm horizontal displacement and ~84 mm uplift.

## 3. Earthquake Source and Slip Distribution Modeling

The Lushan earthquake occurred on the boundary zone between the Tibetan plateau and Sichuan basin. We employ two separate layered media on the two sides of the boundary to represent the crustal structure

(see the supporting information for details), and use the PSGRN/PSCMP code [Wang *et al.*, 2006] to calculate the Green's function of dislocation in a layered elastic media.

We invert for the earthquake source location, geometry, and slip distribution in two steps. We first assume a uniform slip distribution over a rectangular fault plane, integrate point-source Green's functions over the fault plane for the Green's functions of the plane's dislocations, and use a grid search to obtain the optimal fault location and geometry parameters, including latitude, longitude, and depth of the southwest end point of the dislocation's top edge, and strike, length along strike, and downdip width of the fault plane. During each grid-search iteration with a given set of fault location and geometry parameters, the GPS coseismic displacement data are used to invert for the strike and dip components of slip on the fault plane using the weighted least squares method. By comparing the weighted postfit residual  $\chi^2$  values resulting from the grid search, the optimal model parameters are obtained and listed in Table S1. We also use the  $F$  test to evaluate uncertainties of the model parameters (see the supporting information for details and Shen *et al.* [1996] for method). The result shows 22.5 km and 17.0 km for the length and width of the fault plane, striking N28°E and dipping 43° to the NW, with the upper edge located at 7.7 km below the Earth's surface. The centroid point of the fault plane (102.938°E, 30.295°N) is located at 13.5 km depth, which is close to the centroid moment depth obtained by CENC. The uniform slip model shows that the slip is dominated by thrust rupture of 0.70 m, with a minor sinistral component of 0.10 m (i.e., a rake angle of 81.7°). The corresponding seismic moment release is  $8.1 \times 10^{18}$  N·m, equivalent to a Mw6.6 earthquake.

In the next step, we fix the strike, dip, and location of the fault plane at the values given above, enlarge the fault plane, and invert for distributed slip on the fault plane. The fault plane is  $46 \times 38$  km in size with the top edge up to the surface and is meshed into  $23 \times 19$  patches, each  $\sim 2 \times 2$  km in size. A first-order smoothing is imposed on the slip components of neighboring patches, along with zero slip on the boundary patches. These a priori constraints are conditioned with a finite uncertainty, whose amount is determined through balancing the trade-off between the weighted postfit residual  $\chi^2$  of data and the number of parameters resolved by the data in the inversion (see the supporting information for details). The data and the model fitting result are displayed in Figure 1 and listed in the supporting information. As can be seen from Figure 1, most of the predicted displacement vectors fit the observations well, with the corresponding postfit residuals on the order of a couple of millimeters. One exception is the vertical component of site LS06, for which the model overpredicts the datum by 22 mm. Such a deviation is perhaps the result of the lower precision of this observation. Only 6 h data were collected at this station after quake, which makes the estimation of its postseismic position less accurate, particularly for the vertical component affected by the daily fluctuation of the tropospheric delay. The overall model fitting, nevertheless, is very satisfactory.

The resulting slip distribution is shown in Figure 2a and listed in the supporting information, with the seismic moment release estimated as  $9.5 \times 10^{18}$  N·m, equivalent to a Mw6.6 event. This moment estimate is only slightly larger than that of the uniform slip model, with the weighted postfit residual  $\chi^2$  of data reduced from  $\sim 71$  to  $\sim 61$ . Most of the slip is concentrated in a  $\sim 20 \times 15$  km region on the fault plane, with the maximum slip of 0.61 m occurring at a depth of  $\sim 13$  km with a rake angle of 71°. The slips on the fault patches near the surface are less than 0.1 m, and the overall slip pattern shows a gradual decrease of slip from  $\sim 13$  km depth to the surface.

Reliability of the result of the distributed slip model largely relies on its resolution, whose distributions for the strike and dip slip components are shown in Figure 2b. Because of the small fault patch size and smoothing over them, most of the resolutions for individual patches are about 1–3%, with a number of patches near the surface up to 15%. The only meaningful assessment of the solution will have to be through taking average over multiple fault patches whose aggregated resolution is close to or greater than 1. As shown in Figure 2b, the total resolution for the patches with dip-slip  $> 0.45$  m (area A in Figure 2b) is 0.67, and the total resolution for the patches with dip-slip  $> 0.35$  m (area B in Figure 2b) is 2.19, respectively. Resolution distribution for the strike-slip components is similar. We therefore conclude that the pattern of  $> 0.45$  m slip averaged over an area of  $220 \text{ km}^2$  on fault is mostly resolved, and the pattern of  $> 0.35$  m slip averaged over an area of  $620 \text{ km}^2$  is completely resolved.

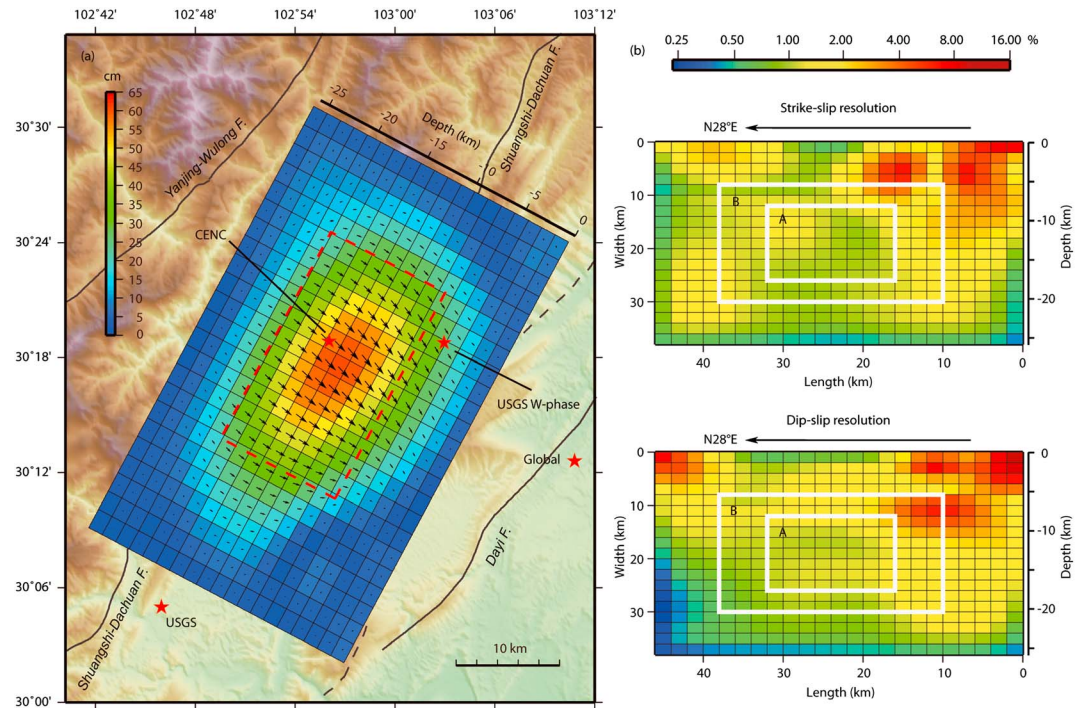


**Figure 2.** (a) Map view of the coseismic slip distribution of the Lushan earthquake. The rectangle outlined by red dashed lines marks the location of the uniform slip fault plane. The stars represent the epicenter locations from multiple sources. (b) Resolution distribution of the strike-slip (upper panel) and dip-slip (lower panel) components.

## 4. Discussion and Conclusions

### 4.1. Fault Slip Near Surface

Our model yields less than 0.1 m slip on the fault patches near the surface. But because finite zero-slip constraints are imposed on the patches at the top edge, it is difficult to tell whether the close-to-zero slip is real or the result of a priori constraints. We perform two test runs to explore whether the rupture reached to shallow depth or even the surface. In the first test (Test One), we release the zero-slip constraints on the top patches while keeping the rest of the model setting and constraints the same (see the supporting information for details). The resulting slip distribution pattern is pretty much the same as before, except that the thrust slip at the surface is increased slightly to about 0.10 ~ 0.15 m for an extent of about 15 km, with uncertainties around 0.07 m. The *F* test shows that the model improvement is at the 90% confidence level. In the second test (Test Two), we cut off the top three-layer of the fault plane and invert for the slip distribution again. The *F* test shows that comparing to the buried fault model without the top three-layer (Test Two), the model with shallow slip (Test One) gains limited improvement in data fitting, and the significance of the improvement is at the 92% confidence level. We conclude from these test results that data favor modest amount of slip near surface, but due to limitation of the data our model cannot unambiguously prove the shallow slip. If shallow slip does exist, it should be no more than 0.1 ~ 0.2 m on the surface and may well be distributed over a finite deformation zone and difficult to identify in the field due to thick sediments and dense vegetation. Such an inference is consistent with the result of geological field survey after the earthquake, which reported distributed fissures and pushed-up cement pavements rather than clear fault surface offsets in the epicentral region [Xu *et al.*, 2013].

### 4.2. Seismogenic Fault

Our uniform slip inversion result indicates that the Lushan earthquake struck an unknown fault along a fold belt located between the Shuangshi-Dachuan and Dayi faults, but neither fault is likely to be responsible for the Lushan earthquake. The surface projection of the inferred fault plane coincides with the eastern foothills of the Longmen Shan range (Figure 3a). A closer look at the local topography reveals that the seismogenic fault is right underneath a small range trending NE (Figure 3b), which was interpreted as an anticline structure

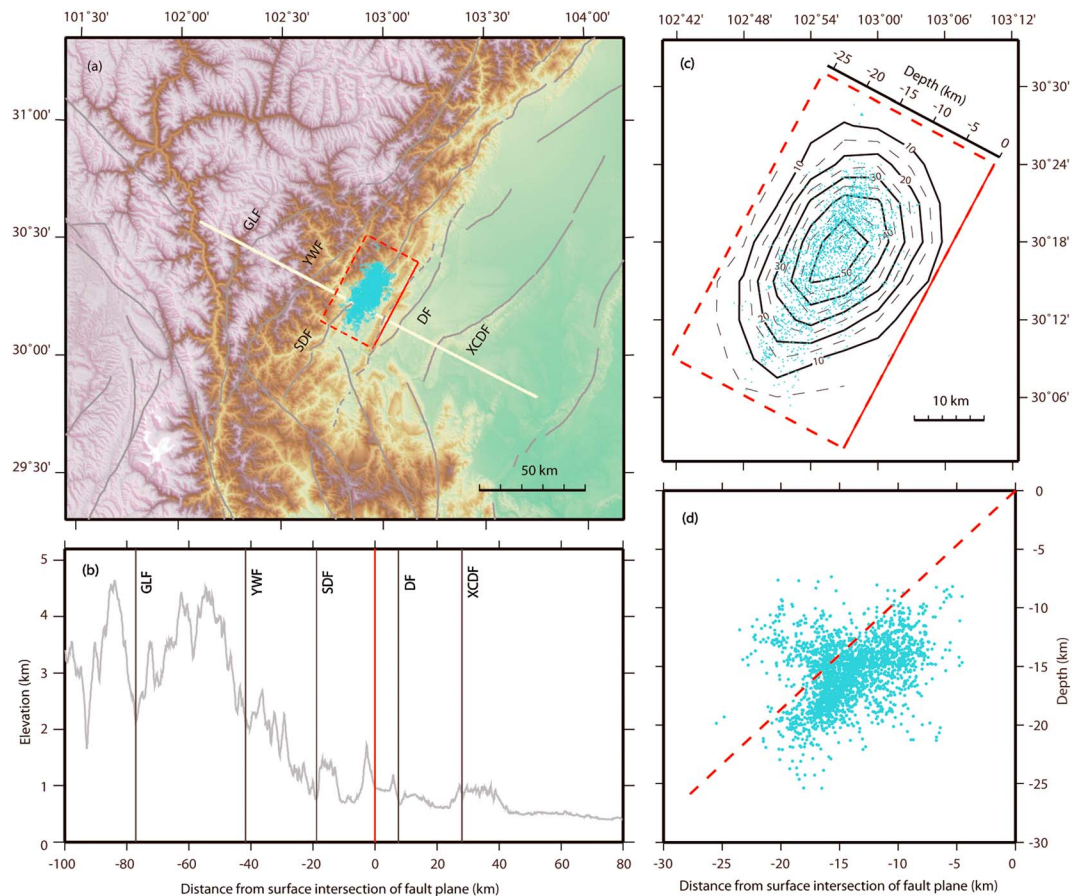


**Figure 3.** Location and geometry of the fault plane of the Lushan earthquake. (a) Surface projection of the fault plane (red rectangle) and aftershocks (blue dots). White line shows the location of topographic profile. Abbreviations are: GLF, Gengda-Longdong Fault; YWF, Yanjing-Wulong Fault; SDF, Shuangshi-Dachuan Fault; DF, Dayi Fault; XCDF, Xinjin-Chengdu-Deyang Fault. (b) Side view of topographic profile versus distance from surface projection of the fault plane (red line). The curve represents the elevation along the profile. (c) Surface projection of contoured slip model on the fault plane and the aftershocks. The contours of slip are in cm. (d) Side view of the model fault plane and the aftershocks.

[Xu *et al.*, 2013]. Based on aftershock distribution and its location with respect to the anticline, Xu *et al.* [2013] envision that, similar to the 1983 Coalinga and 1987 Whittier Narrows earthquakes in California, the Lushan earthquake occurred on a propagating blind thrust fault underneath this growing fold. The buried slip distribution of our fault slip model and its apparent association with the surface morphology seem to lend support to Xu *et al.*'s inference. Previously identified faults in the region as shown in Figures 3a and 3b, however, cannot be the seismogenic fault of this quake since the peak surface deformation area is away from these faults.

#### 4.3. Fault Geometry and Properties

We also examine the geometry of the inferred fault plane by comparing it with the aftershock distribution. The relocated aftershock locations [Xu *et al.*, 2013] coincide well with the high-slip area of our solution in map view (Figure 3c), indicating postseismic adjustments of the stress field around the fault rupture. This phenomenon is similar to the observation of the 2008 Wenchuan earthquake, whose high-slip zones were found to overlap with concentration regions of aftershocks [Chen *et al.*, 2009; Shen *et al.*, 2009]. Fault structure and rupture dynamics of the Longmen Shan fault zone are therefore, perhaps quite different from many other known fault systems struck by large earthquakes, which commonly show aftershocks to be most abundant outside of the high-slip zone [e.g., Das and Henry, 2003; Lay *et al.*, 2005; Ozawa *et al.*, 2011]. Such a marked difference may reflect a fundamental difference in seismo-tectonic setting. Most of the earthquakes studied in the past are subduction zone or continental strike-slip events, and the interfaces of these seismogenic faults usually had accumulated kilometer level of slip by the time of the earthquake and were

relatively smooth. Continental thrust faults, such as the Longmen Shan fault zone, however, may have less finite slip and continue to evolve and mature before faulting reaches to the Earth's surface. The interface of the Longmen Shan fault zone therefore might be much more discontinuous and rough compared to mature subduction zone and continental strike-slip faults [Sagy *et al.*, 2007]. Such evolving fault zones may be expected to develop more distributed fracturing and aftershocks along the high-slip zones of the earthquake rupture.

#### 4.4. Fault Depth

A side view of the aftershocks and the fault plane shows good alignment but also illustrates a systematic offset of ~2 km, with most aftershocks located in the footwall of the model rupture (Figure 3d). Such an offset could arise from a setting error of the initial reference depth in the double-differencing method or error in the seismic velocity model used for relocation of the aftershocks. Inaccurate elastic media model used in our study could also introduce bias, but that is expected to be less than that from the aftershock relocation since our model has taken into account the first-order effect of layering and lateral variation in the media.

#### 4.5. Sinistral Slip Component

Our inversion result shows that rupture of the Lushan earthquake is dominated by thrust faulting, accompanied by a significant sinistral component. The peak slip has 0.57 m thrust and 0.20 m sinistral motion, respectively, with a rake angle of 71°. This result is markedly different from most of the seismic results such as the Global CMT, CENC CMT, and USGS W-phase CMT solutions, which showed a minor dextral component, but agrees with the USGS CMT solution, which indicated a sinistral component. Previous tectonic and geodetic studies also indicated that the Longmen Shan fault system, in general, deforms with a shortening rate of 1 ~ 2 mm/a and a dextral rate of ~1 mm/a [e.g., Densmore *et al.*, 2007; Burchfiel *et al.*, 2008; Shen *et al.*, 2005]. To assess reliability of the sinistral slip component, we perform a series of test runs, and the results support our current model and rule out confidently the possibility that rupture did not have a sinistral component (see the supporting information for more details).

#### 4.6. Regional Tectonic Deformation Pattern

To understand the sinistral slip of the Lushan earthquake, we also take a closer look at the geodetic data for assessment of the interseismic deformation pattern of the region. In an analysis of the GPS velocity field, Wang *et al.* [2008] inferred sinistral slip across the southern end of the Longmen Shan fault. We plot the same GPS data in the region on profiles (Figure S7), which reveals that besides shortening across the Longmen Shan fault, there is ~1.0 mm/a dextral slip across a fault segment north of Lushan. The GPS data in the near field across a profile south of Lushan are scarce and show no clear sense of strike-slip motion, but the data in the intermediate field west of the Longmen Shan fault demonstrate significant sinistral motion (Figure S7). The Lushan earthquake is located close to a triple junction between the Xianshuihe, Anninghe, and Longmen Shan faults. Block motion models derived from the GPS velocity field predict sinistral slip across the Xianshuihe and Anninghe faults, and dextral and thrust motion across the Longmen Shan fault, respectively [Meade, 2007; Thatcher, 2007; Wang *et al.*, 2008]. Such a model, however, seems no longer adequate to describe the crustal deformation field in the region near the fault triple junction. Instead, the regional crust is perhaps fragmented, with more secondary faults coming into play due to a buttressing effect at the triple junction. The deformation field is distributed and continuous, with a gradual transition of the faulting mechanism from north to south, from a modest dextral slip (~1 mm/a) on the Longmen Shan fault to dominantly sinistral slip (~8 mm/a) on the Anninghe-Daliangshan fault system. The Lushan earthquake mechanism may reflect this fault kinematic transition near the triple junction. The strike of the Lushan fault rupture is NNE, which is between the NE strike of the Longmen Shan fault and the N-S strike of the Anninghe fault, providing another piece of evidence for the distributed deformation and transition of the faulting mechanism.

Based on these observations, we envision that the Longmen Shan fault system at its southern end spans a broad region, where multiple fault strands are seismically active and interact with the Xianshuihe fault to the west and the Anninghe fault to the south. This system accommodates the transition from eastward extrusion in the north to southeastward extrusion and sinistral strike-slip shear in the south along the eastern margin of the Tibetan plateau.

### Acknowledgments

We appreciate review comments by Christodoulos Kyriakopoulos and an anonymous reviewer, which greatly improved the manuscript. This work is financially supported by the National Science Foundation of China (41090294 and 41274008).

The Editor thanks Christodoulos Kyriakopoulos and an anonymous reviewer for their assistance in evaluating this paper.

### References

- Burchfiel, B. C., Z. Chen, Y. Liu, and L. H. Royden (1995), Tectonics of the Longmen Shan and adjacent regions, *Int. Geol. Rev.*, *37*, 661–735.
- Burchfiel, B. C., L. H. Royden, R. D. van der Hilst, Z. Chen, R. W. King, C. Li, J. Lü, H. Yao, and E. Kirby (2008), A geological and geophysical context for the Wenchuan earthquake of 12 May 2008, Sichuan, People's Republic of China, *GSA Today*, *18*, 4–11, doi:10.1130/GSATG18A.1.
- Chen, J. H., Q. Y. Liu, S. C. Li, B. Guo, Y. Li, J. Wang, and S. H. Qi (2009), Seismotectonics study by relocation of the Wenchuan Ms8.0 Earthquake sequence (in Chinese), *Chin. J. Geophys.*, *52*(2), 390–397.
- Chen, Z., B. C. Burchfiel, Y. Liu, R. W. King, L. H. Royden, W. Tang, E. Wang, J. Zhao, and X. Zhang (2000), Global Positioning System measurements from eastern Tibet and their implications for India/Eurasia intercontinental deformation, *J. Geophys. Res.*, *105*(B7), 16,215–16,227, doi:10.1029/2000JB900092.
- Das, S., and C. Henry (2003), Spatial relation between main earthquake slip and its aftershock distribution, *Rev. Geophys.*, *41*(3), 1013, doi:10.1029/2002RG000119.
- Densmore, A. L., M. A. Ellis, Y. Li, R. Zhou, G. S. Hancock, and N. Richardson (2007), Active tectonics of the Beichuan and Pengguan faults at the eastern margin of the Tibetan Plateau, *Tectonics*, *26*, TC4005, doi:10.1029/2006TC001987.
- King, R. W., F. Shen, B. C. Burchfiel, L. H. Royden, E. Wang, Z. Chen, Y. Liu, X. Zhang, J. Zhao, and Y. Li (1997), Geodetic measurement of crustal motion in southwest China, *Geology*, *25*(2), 179–182, doi:10.1130/0091-7613.
- Lay, T., et al. (2005), The great Sumatra-Andaman earthquake of 26 December 2004, *Science*, *308*(5725), 1127–1133, doi:10.1126/science.1112250.
- Ma, B., G. Su, Z. Hou, and S. Shu (2005), Late Quaternary slip rate in the central part of the Longmenshan Fault Zone from terrace deformation along the Minjiang River (in Chinese), *Seismol. Geol.*, *27*, 234–242.
- Meade, B. J. (2007), Present-day Kinematics at the India-Asia collision zone, *Geology*, *35*, 81–84, doi:10.1130/G22924A.1.
- Ozawa, S., T. Nishimura, H. Suito, T. Kobayashi, M. Tobita, and T. Imakiire (2011), Coseismic and postseismic slip of the 2011 magnitude-9 Tohoku-Oki earthquake, *Nature*, *475*, 373–377, doi:10.1038/nature10227.
- Sagy, A., E. E. Brodsky, and G. J. Axen (2007), Evolution of fault-surface roughness with slip, *Geology*, *35*(3), 283–286, doi:10.1130/G23235A.1.
- Shen, Z.-K., B. X. Ge, D. D. Jackson, D. Potter, M. Cline, and L. Y. Sung (1996), Northridge earthquake rupture models based on the global positioning system measurements, *Bull. Seismol. Soc. Am.*, *86*(1B), S37–S48.
- Shen, Z.-K., J. Lu, M. Wang, and R. Burgmann (2005), Contemporary crustal deformation around southeast borderland of Tibetan plateau, *J. Geophys. Res.*, *110*, B11409, doi:10.1029/2004JB003421.
- Shen, Z.-K., J. B. Sun, P. Z. Zhang, Y. G. Wan, M. Wang, R. Burgmann, Y. H. Zeng, W. J. Gan, H. Liao, and Q. L. Wang (2009), Slip maxima at fault junctions and rupturing of barriers during the 2008 Wenchuan earthquake, *Nat. Geosci.*, *2*, 718–724, doi:10.1038/ngeo636.
- Thatcher, W. (2007), Microplate model for the present-day deformation of Tibet, *J. Geophys. Res.*, *112*, B01401, doi:10.1029/2005JB004244.
- Wang, R., F. Lorenzo-Martin, and F. Roth Frank (2006), PSGRN/PSCMP—a new code for calculating co- and post-seismic deformation, geoid and gravity changes based on the viscoelastic-gravitational dislocation theory, *Comput. Geosci.*, *32*, 527–541.
- Wang, W. M., J. L. Hao, and Z. X. Yao (2013), Preliminary result for rupture process of Apr. 2, 2013, Lushan Earthquake, Sichuan, China (in Chinese), *Chin. J. Geophys.*, *56*(4), 1412–1417, doi:10.6038/cjg20130436.
- Wang, Y. Z., et al. (2008), GPS-constrained inversion of present-day slip rates along major faults of the Sichuan-Yunnan region, China, *Sci. China Earth Sci.*, *51*(9), 1267–1283.
- Xu, X. W., X. Z. Wen, G. H. Yu, G. H. Chen, Y. Klinger, J. Hubbard, and J. Shaw (2009), Co-seismic reverse- and oblique-slip surface faulting generated by the 2008 Mw 7.9 Wenchuan earthquake, China, *Geology*, *37*(6), 515–518, doi:10.1130/G25462A.1.
- Xu, X. W., et al. (2013), Lushan Ms7.0 earthquake: A blind reverse-fault earthquake (in Chinese), *Chin. Sci. Bull.*, *58*, doi:10.1007/s11434-013-5999-4.
- Zeng, X. F., Y. Luo, L. B. Han, and Y. L. Shi (2013), Lushan Ms7.0 earthquake on 20 April 2013: A high-angle thrust event (in Chinese), *Chin. J. Geophys.*, *56*(4), 1418–1421, doi:10.6038/cjg20130437.
- Zhang, P. Z., X. W. Xu, X. Z. Wen, and Y. K. Ran (2008), Slip rate and recurrence intervals of the Longmen Shan active fault zone, and tectonic implications for the mechanism of the May 12 Wenchuan earthquake, 2008, Sichuan, China (in Chinese), *Chin. J. Geophys.*, *51*(4), 1066–1073.
- Zhang, Y., L. S. Xu, and Y. T. Chen (2013), Rupture process of the Lushan 4.20 earthquake and preliminary analysis on the disaster-causing mechanism (in Chinese), *Chin. J. Geophys.*, *56*(4), 1408–1411, doi:10.6038/cjg20130435.